

Large anomalous Hall effect in the kagome ferromagnet LiMn_6Sn_6

Dong Chen,^{1,2,*} Congcong Le,¹ Chenguang Fu,^{1,3} Haicheng Lin,¹ Walter Schnelle,¹ Yan Sun,¹ and Claudia Felser¹

¹Max Planck Institute for Chemical Physics of Solids, 01187 Dresden, Germany

²College of Physics, Qingdao University, Qingdao 266071, China

³State Key Laboratory of Silicon Materials, and School of Materials Science and Engineering, Zhejiang University, Hangzhou 310027, China

Kagome magnets are believed to have numerous exotic physical properties due to the possible interplay between lattice geometry, electron correlation and band topology. Here, we report the large anomalous Hall effect in the kagome ferromagnet LiMn_6Sn_6 , which has a Curie temperature of 382 K and easy plane along with the kagome lattice. At low temperatures, unsaturated positive magnetoresistance and opposite signs of ordinary Hall coefficient for ρ_{xz} and ρ_{yx} indicate the coexistence of electrons and holes in the system. A large intrinsic anomalous Hall conductivity of $380 \Omega^{-1} \text{ cm}^{-1}$, or $0.44 e^2/h$ per Mn layer, is observed in σ_{xy}^A . This value is significantly larger than those in other RMn_6Sn_6 (R = rare earth elements) kagome compounds. Band structure calculations show several band crossings, including a spin-polarized Dirac point at the K point, close to the Fermi energy. The calculated intrinsic Hall conductivity agrees well with the experimental value, and shows a maximum peak near the Fermi energy. We attribute the large anomalous Hall effect in LiMn_6Sn_6 to the band crossings closely located near the Fermi energy.

I. INTRODUCTION

The magnet with kagome lattice has been studied for a long time in the condensed matter physics and material science communities [1–3]. Kagome lattice is a two-dimensional honeycomb network of corner-sharing triangles. Owing to this special lattice geometry, a band structure with Dirac cones and a flat band has been revealed by the simple tight-binding model [4]. Embodied with magnetism and spin-orbit coupling (SOC), some kagome magnets have been recently found to have exotic topological states and phenomena. For example, the spin-polarized Dirac cone with a spin-orbit-coupling induced gap has been observed in kagome ferromagnet Fe_3Sn_2 [5]. Giant intrinsic anomalous Hall effect caused by the large Berry curvature have been observed in antiferromagnets Mn_3Sn , Mn_3Ge [6–8], and the magnetic Weyl semimetal $\text{Co}_3\text{Sn}_2\text{S}_2$ [9, 10]. These experimental breakthroughs indicate that kagome magnet is a promising system for investigating the interplay of lattice geometry, electron correlation, and band topology.

Recently, another kagome magnet family RMn_6Sn_6 (R = trivalent rare earth elements) also has received much attention [11–14]. They have the same layered hexagonal structure (space group $P6/mmm$), which is composed by kagome Mn_3 layers alternatively inserted by RSn_2 and Sn_4 layers. All the members are magnetic ordered with relatively high transition temperatures [15–18]. Among these materials, TbMn_6Sn_6 , with a ferrimagnetic order perpendicular to the kagome lattice, was found to have the Chern gapped Dirac fermions [11]. Antiferromagnetic YMn_6Sn_6 was found to exhibit giant topological Hall effect near room temperature [12]. Although with multiple magnetic structures and fascinating properties, ferromagnetism is absent in RMn_6Sn_6 family and the discovered anomalous Hall effect among them is not impressive. Actually, the R elements can be completely replaced by Li, Mg, or Ca, and the magnetism of the new systems are all ferromag-

netic [19, 20]. In the meantime, the lower valences of Li, Mg, and Ca also reduce the system's number of valence electrons. Thus, the simultaneously tuned magnetic and electronic states in these new “166” compounds give us a chance to pursue larger anomalous Hall effect and other new phenomena.

In this paper, we report a study on the magnetotransport properties of LiMn_6Sn_6 , a member of the “166” material family with minimal number of valence electrons. This compound is a ferromagnet with the Curie temperature (T_C) of 382 K and has an easy plane parallel to the kagome lattice (ab plane). The resistivity shows a metallic temperature dependence, and the low-temperature magnetoresistance is positive and has no tendency to saturate below 9 T. Hall resistivity shows opposite signs in the ordinary Hall coefficient of ρ_{xz} and ρ_{yx} , indicating the coexistence of electrons and holes in the system. A large intrinsic contribution in the anomalous Hall conductivity (AHC) of $380 \Omega^{-1} \text{ cm}^{-1}$, or $0.44 e^2/h$ per Mn layer, can be obtained, which is much larger than those in the RMn_6Sn_6 compounds. By band structure calculations, we find several linear band crossings and a small density of states (DOS) near the E_F . At the K point of the Brillouin zone, we find a spin-polarized Dirac dispersion close to the E_F . The energy dependent intrinsic AHC calculated from Berry curvature has a maximum peak near the E_F with the peak value close to the experimental one. These results show that the large anomalous conductivity in LiMn_6Sn_6 is related to the band crossings near the E_F .

II. EXPERIMENT AND METHODS

The single crystals of LiMn_6Sn_6 were grown by self-flux method. Li, Mn, and Sn with atomic ratio of Li : Mn : Sn = 3 : 3 : 10 were loaded in a Ta crucible, and a Ta filter with drilled holes was then knocked into the crucible. The crucible was finally arc welded with a Ta cap and sealed in an evacuated quartz tube. The tube was heated to 1000 °C, kept for 20 hours, and then cooled down to 500 °C with a rate of 3 °C/h. After that, the tube was centrifuged to separate the crystals from flux. Hexagonal plate-shaped single

* Dong.Chen@cpfs.mpg.de

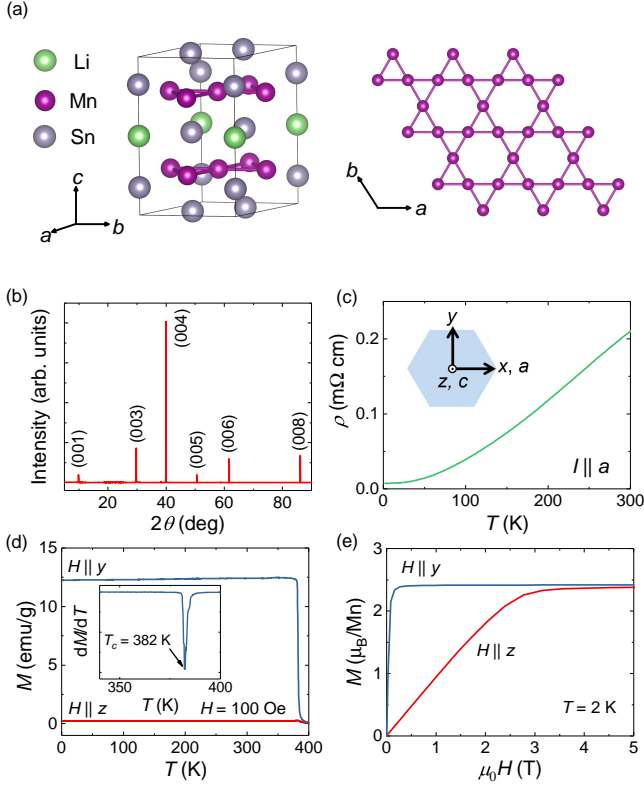


FIG. 1. (a) Crystal structure of LiMn_6Sn_6 . (b) XRD pattern of a LiMn_6Sn_6 single crystal with $(00l)$ reflections. (c) Temperature dependence of resistivity with current along a axis. The inset illustrates the definition of a Cartesian coordinate system based on the hexagonal lattice. (d) Temperature dependence of the magnetization under magnetic field of $H = 100$ Oe lying in and perpendicular to the ab plane. The inset shows the derivative of the magnetization dM/dT vs. T for $H \parallel y$. (e) The isothermal magnetization at $T = 2$ K for $H \parallel y$ and $H \parallel z$.

crystals were obtained without significant air sensitivity. The crystal structure of the samples was checked by x-ray diffraction (XRD) on a PANalytical diffractometer with $\text{Cu } K\alpha$ radiation at room temperature. The hexagonal plate-shaped crystals were used for the magnetic properties measurements, and were cut into sticks before the electrical transport measurements. The magnetic properties and electrical transport properties were measured on a Quantum Design Magnetic Properties Measurement System (MPMS) and a Physical Properties Measurement System (PPMS), respectively.

Our calculations were performed using density functional theory (DFT) as implemented in the Vienna ab initio simulation package (VASP) code [21–23]. The generalized-gradient approximation (GGA) for the exchange correlation functional was used. Throughout the work, the cutoff energy was set to be 550 eV for expanding the wave functions into plane-wave basis. In the calculation, the Brillouin zone was sampled in the k space within Monkhorst-Pack scheme [24]. On the basis of the equilibrium structure, the k mesh used was $10 \times 10 \times 6$. The intrinsic Hall conductivity σ_{xy}^{int} is obtained by integrating the z component of Berry curvature $\Omega_{xy}^z(\mathbf{k})$ on all the occupied

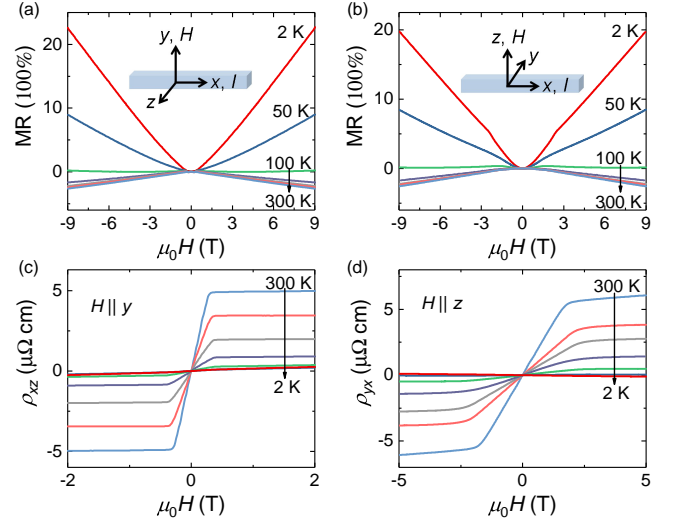


FIG. 2. (a, b) Magnetic field dependence of magnetoresistance at various temperatures measured with $H \parallel y$ and $H \parallel z$, respectively. The insets show the corresponding measurement geometries. (c, d) Magnetic field dependence of Hall resistivity at various temperatures with the same measurement geometries with (a) and (b), respectively.

states through the Brillouin zone with SOC included and the moment of Mn along z axis.

III. RESULTS AND DISCUSSION

LiMn_6Sn_6 has the same crystal structure with the RMn_6Sn_6 compounds, with lattice parameters of $a = b = 5.497$ Å, $c = 9.026$ Å. As shown in Fig. 1(a), the Mn kagome lattice is parallel to the ab plane. Figure 1(b) shows the XRD pattern of the hexagonal surface of a plate-like single crystal. All the peaks can be identified as the $(00l)$ reflections of LiMn_6Sn_6 as labeled on the pattern, indicating the (001) surface of the crystal. The phase of the samples was further checked by the powder XRD. Figure 1(c) shows the temperature dependence of the resistivity with current flowing along a axis. It has a metallic behavior with a residual resistivity ratio $\rho(300 \text{ K})/\rho(2 \text{ K}) = 29$. The inset of Fig. 1(c) defines a Cartesian coordinate system for later using, with $x \parallel a$, $z \parallel c$, and $y \perp x, z$. The ferromagnetism of the sample can be illustrated by the temperature dependence of magnetization with magnetic field $H = 100$ Oe along with the ab plane ($H \parallel y$) and the c axis ($H \parallel z$) [Fig. 1(d)]. The magnetization for $H \parallel y$ is much larger than that for $H \parallel z$ below T_C , suggesting the ab plane is the easy plane. The T_C can be determined by the peak of the derivative of magnetization dM/dT for $H \parallel y$, as shown in the inset of Fig. 1(d), which gives $T_C = 382$ K. Figure 1(e) shows the isothermal magnetization curves at $T = 2$ K for the two directions. Due to the easy-plane anisotropy and the high quality of the crystals, there is no hysteresis in the magnetization curve. The saturation magnetization is about $2.4 \mu_B/\text{Mn}$. All the magnetic properties are consistent with those previously revealed by neutron scattering experiment [19].

Figures 2(a) and (b) show the magnetic field dependence of the MR with the measurement geometries illustrated in the corresponding insets. The current is always along x axis, and the magnetic field is along y and z axis, respectively. The MR for $H \parallel y$ shows a parabolic-like field dependence at $T = 2$ K, and has no tendency to saturate below 9 T. For $H \parallel z$, the MR at low temperatures show a kink around 2 T, and has a nearly linear behavior in higher field. With temperature increases, the MR for both directions gradually decline and become negative when temperature higher than 100 K. As a ferromagnetic metal, the negative MR of LiMn_6Sn_6 at high temperature can be understood as the consequence of suppressed spin-disorder scattering. While at low temperature, the positive MR indicates that some other mechanisms dominate in the transport process.

To extract more information in the transport process, we performed the Hall effect measurements. Figures 2(c) and (d) show the field dependence of the Hall resistivity ρ_{xz} and ρ_{yx} for $H \parallel y$ and $H \parallel z$, respectively, which are defined as $\rho_{xz} = -E_z/j_x$ and $\rho_{yx} = E_y/j_x$. At high temperatures, the Hall resistivity in both directions exhibit obvious anomalous Hall effect. Conventionally, the Hall resistivity of ferromagnets can be expressed as $\rho_H = \rho_H^0 + \rho_H^A = R_0 B + R_s \mu_0 M$, where ρ_H^0 (ρ_H^A) and R_0 (R_s) are the ordinary (anomalous) Hall resistivity and coefficient, respectively. It can be seen that the anomalous Hall resistivity has different saturation fields with the magnetization curves shown in Fig. 1(e), especially for $H \parallel y$. This is caused by the different magnetization factors that come from the different sample shapes in the two measurements. The ordinary Hall resistivity shows different slopes in the two directions. This is more obvious at lower temperatures. At 2 K, the anomalous Hall resistivity becomes too weak to be observed due to the reduction of resistivity, and the ordinary Hall resistivity is dominant. At this temperature, the slope of Hall resistivity is positive for ρ_{xz} while negative for ρ_{yx} , which means that holes (electrons) are dominant for $H \parallel y$ ($H \parallel z$). This phenomenon reflects the coexistence of both holes and electrons in this compound, and the densities can be tuned by the direction of magnetic field. The coexistence of holes and electrons may explain the positive unsaturated MR at low temperature, which may be caused by the compensation effect of the two types of carrier [25].

The anomalous Hall effect in ferromagnetic conductor is considered to come from three different contributions, and the AHC can be expressed as $\sigma_H^A = \sigma_{int} + \sigma_{sk} + \sigma_{sj}$, where σ_{int} is the intrinsic contribution, and σ_{sk} and σ_{sj} are the parts come from screw scattering and side jump mechanisms, respectively [26]. Both of the σ_{sk} and σ_{sj} terms are the consequences of extrinsic scattering from disorder or impurities, while the σ_{int} term depends only on the band structure. Figures 3(a) and (b) show the anomalous parts of the Hall conductivity σ_{zx}^A and σ_{xy}^A , respectively, which are obtained by $\sigma_{ij}^A = \rho_{ji}^A/(\rho_{ji}^2 + \rho_{ii}^2)$. To extract the intrinsic contribution of the AHC, we employ the so-called Tian-Ye-Jin (TYJ) scaling [5, 27]: $\sigma_{xy}^A = a\sigma_{xx}^2 + \sigma_{xy}^{int}$, where a is a system relevant constant, and σ_{xy}^{int} is the intrinsic AHC contribution. Figures 3(c) and (d) show the AHC as the function of σ_{xx}^2 for the two directions. The intrinsic contribution of AHC can be

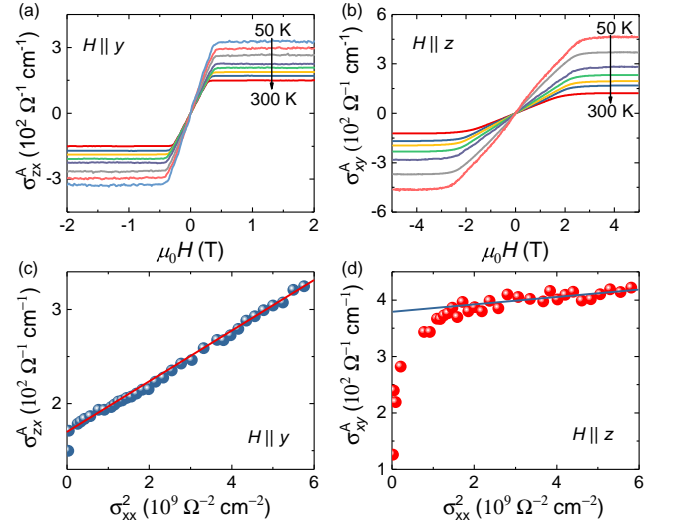


FIG. 3. (a, b) Anomalous part of the Hall conductivity σ_{zx}^A and σ_{xy}^A as the function of magnetic field at various temperatures measured with $H \parallel y$ and $H \parallel z$, respectively. (c, d) The anomalous Hall conductivity σ_{zx}^A and σ_{xy}^A versus σ_{xx}^2 with fitting lines, respectively.

TABLE I. Comparison of the intrinsic AHC of LiMn_6Sn_6 with those of RMn_6Sn_6 , where FIM denotes the ferrimagnet and FM is the ferromagnet.

	Magnetic order	σ_{xy}^{int} (e^2/h per Mn layer)	Reference
Gd	FIM	0.27, 0.17	[13, 14]
Tb	FIM	0.14	[11, 14]
Dy	FIM	0.07	[14]
Ho	FIM	0.13	[14]
Er	FIM	0.04	[14]
Li	FM	0.44	This work

obtained from the intercept of the fitting line, which is $170 \Omega^{-1} \text{cm}^{-1}$ and $380 \Omega^{-1} \text{cm}^{-1}$ for σ_{zx}^{int} and σ_{xy}^{int} , respectively. This anisotropic intrinsic AHC suggests the influence of magnetic field direction on the electronic structure of LiMn_6Sn_6 again. The value of σ_{xy}^{int} can be converted into $0.88 e^2/hc$, where c is the cross-plane lattice constant. Considering there are two kagome Mn layers in a unit cell, it gives $0.44 e^2/h$ per Mn layer. This intrinsic Hall conductivity component in LiMn_6Sn_6 is much larger than those that have been found in the RMn_6Sn_6 compounds with ferrimagnetic order, such as $0.27 e^2/h$ per Mn layer for GdMn_6Sn_6 , and $0.14 e^2/h$ per Mn layer for TbMn_6Sn_6 , as listed in Table I.

Because σ_{int} depends only on the band structure, we carried out the first-principles calculations to have a better understanding of the large σ_{xy}^{int} in LiMn_6Sn_6 . Figure 4 (a) shows the band structure without SOC in the vicinity of E_F . Both spin-up and spin-down bands pass through the E_F , with several crossings close to the E_F . If the SOC is included into account, the band structure is almost unaltered due to the light elements, only with some small gaps opened in the band crossings. This band structure is consistent with the two types of carriers revealed by the Hall measurements. It is worth point-

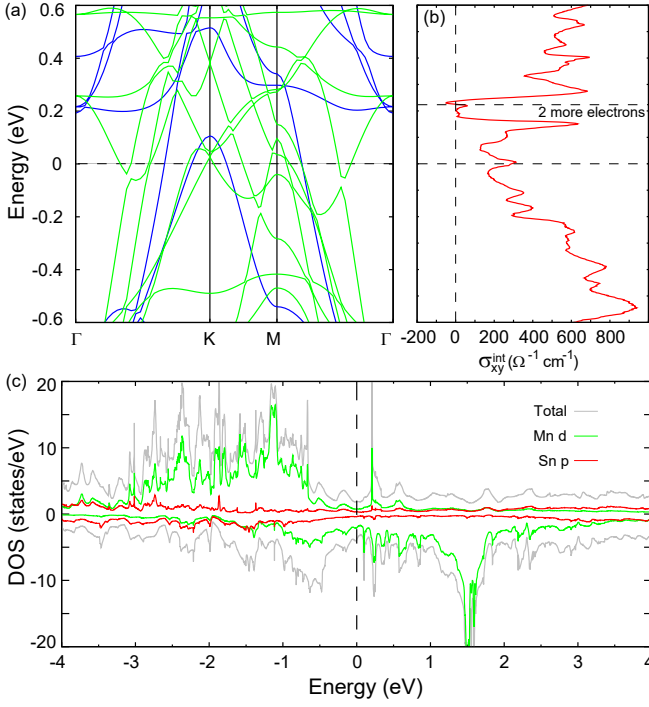


FIG. 4. (a) The band structure of LiMn₆Sn₆ without SOC. The spin-up bands appear in blue lines, and the spin-down bands appear in green lines. (b) Energy dependence of the intrinsic AHC σ_{xy}^{int} , with the E_F of LiMn₆Sn₆ is 0. The upper dashed line denotes the lifted E_F with extra 2 electrons per formula unit. (c) Spin-resolved total and orbital-projected densities of states in the vicinity of E_F .

ing out that there is a spin-polarized linear crossing slightly above the E_F at the K point, and it is gapped with the consideration of SOC. This is reminiscent of the Chern gapped Dirac fermions found in TbMn₆Sn₆ [11]. Figure 4(c) shows the spin-resolved density of states near the E_F . The bands near the E_F are mainly hybridized by the Mn-*d* and Sn-*p* orbitals. The DOS for both directions have relatively small values at the E_F , consistent with the several band crossings near the E_F revealed by the band structure. The calculated magnetic moment based on the spin-resolved DOS is 2.4 μ_B/Mn , same with the value obtained in the magnetization curves. The energy dependence of intrinsic AHC σ_{xy}^{int} can be calculated from Berry curvature based on the band calculations. As shown in Fig. 4 (b), there is a peak near the E_F with the value at E_F of 300 $\Omega^{-1} \text{cm}^{-1}$, which is close to the experimental value. In the time-reversal-symmetry-broken systems, a band crossing near the E_F with a SOC induced gap is believed to contribute

a large Berry curvature [28]. Thus, the peak of σ_{xy}^{int} near E_F can be understood as the consequence of the close positions of the band crossings to the E_F . We can also notice a higher peak of σ_{xy}^{int} centered at about 0.15 eV, which is followed by a deep valley around 0.2 eV. If we assume the RMn₆Sn₆ compounds have similar band structure, the E_F can be lifted for about 0.23 eV by the 2 extra valence electrons of *R*. This results in the smaller σ_{xy}^{int} in RMn₆Sn₆, as shown by the upper dashed line in Fig. 4(b). All the calculation results fit well with the experimental observations, suggesting the reliability of our calculations. Based on the calculations, a much larger AHC up to 0.73 e^2/h per Mn layer can be expected if the ferromagnetic compounds with E_F located at about 0.15 eV can be synthesized, such as (Li, *R*)Mn₆Sn₆ and (Mg, *R*)Mn₆Sn₆.

IV. CONCLUSION

In conclusion, we have investigated the magnetic, transport properties, and band structure of LiMn₆Sn₆, which is a ferromagnet with $T_C = 382$ K and the easy plane along its kagome lattice. With $H \parallel y$ and $H \parallel z$, LiMn₆Sn₆ shows nonsaturated positive MR and opposite ordinary Hall coefficients at low temperatures, suggesting the coexistence of electrons and holes. An intrinsic Hall conductivity component of 380 $\Omega^{-1} \text{cm}^{-1}$ can be found in σ_{xy}^A , which is much larger than those in the ferrimagnetic RMn₆Sn₆ compounds. First principles calculations reveal several band crossings including a spin-polarized Dirac dispersion, a minimum DOS, and a maximum intrinsic AHC near the E_F . All of these results suggest the relationship between the large intrinsic anomalous Hall effect with the band crossings near the E_F .

V. ACKNOWLEDGMENTS

This work was supported by the European Research Council Advanced Grant (No. 742068) “TOPMAT”, the European Union’s Horizon 2020 Research and Innovation Programme (No. 824123) “SKYTOP”, the European Union’s Horizon 2020 Research and Innovation Programme (No. 766566) “ASPIN”, the Deutsche Forschungsgemeinschaft (Project-ID No. 258499086) “SFB 1143”, the Deutsche Forschungsgemeinschaft (Project-ID No. FE 633/30-1) “SPP Skyrmions”, and the DFG through the Würzburg-Dresden Cluster of Excellence on Complexity and Topology in Quantum Matter ct.qmat (EXC 2147, Project-ID No. 39085490).

[1] T.-H. Han, J. S. Helton, S. Chu, D. G. Nocera, J. A. Rodriguez-Rivera, C. Broholm, and Y. S. Lee, *Nature* **492**, 406 (2012).
[2] S. Depenbrock, I. P. McCulloch, and U. Schollwöck, *Phys. Rev. Lett.* **109**, 067201 (2012).
[3] S. Sachdev, *Phys. Rev. B* **45**, 12377 (1992).
[4] K. Ohgushi, S. Murakami, and N. Nagaosa, *Phys. Rev. B* **62**, R6065 (2000).

[5] L. Ye, M. Kang, J. Liu, F. Von Cube, C. R. Wicker, T. Suzuki, C. Jozwiak, A. Bostwick, E. Rotenberg, D. C. Bell, L. Fu, R. Comin, and J. G. Checkelsky, *Nature* **555**, 638 (2018).
[6] J. Kübler and C. Felser, *EPL* **108**, 67001 (2014).
[7] S. Nakatsuji, N. Kiyohara, and T. Higo, *Nature* **527**, 212 (2015).
[8] A. K. Nayak, J. E. Fischer, Y. Sun, B. Yan, J. Karel, A. C. Komarek, C. Shekhar, N. Kumar, W. Schnelle, J. Kübler, C.

- Felser, S. S. P. Parkin, *Sci. Adv.* **2**, e1501870 (2016).
- [9] E. Liu, Y. Sun, N. Kumar, L. Muechler, A. Sun, L. Jiao, S.-Y. Yang, D. Liu, A. Liang, Q. Xu, J. Kroder, V. Süß, H. Borrmann, C. Shekhar, Z. Wang, C. Xi, W. Wang, W. Schnelle, S. Wirth, Y. Chen, S. T. B. Goennenwein, and C. Felser, *Nat. Phys.* **14**, 1125 (2018).
- [10] Q. Wang, Y. Xu, R. Lou, Z. Liu, M. Li, Y. Huang, D. Shen, H. Weng, S. Wang, and H. Lei, *Nat. Commun.* **9**, 3681 (2018).
- [11] J.-X. Yin, W. Ma, T. A. Cochran, X. Xu, S. S. Zhang, H.-J. Tien, N. Shumiya, G. Cheng, K. Jiang, B. Lian, Z. Song, G. Chang, I. Belopolski, D. Multer, M. Litskevich, Z.-J. Cheng, X. P. Yang, B. Swidler, H. Zhou, H. Lin, T. Neupert, Z. Wang, N. Yao, T.-R. Chang, S. Jia, and M. Z. Hasan, *Nature* **583**, 533 (2020).
- [12] Q. Wang, K. J. Neubauer, C. Duan, Q. Yin, S. Fujitsu, H. Hosono, F. Ye, R. Zhang, S. Chi, K. Krycka, H. Lei, and P. Dai, *Phys. Rev. B* **103**, 014416 (2021).
- [13] T. Asaba, S. M. Thomas, M. Curtis, J. D. Thompson, E. D. Bauer, and F. Ronning, *Phys. Rev. B* **101**, 174415 (2020).
- [14] W. Ma, X. Xu, J.-X. Yin, H. Yang, H. Zhou, Z. Cheng, Y. Huang, Z. Qu, F. Wang, M. Z. Hasan, and S. Jia, *Phys. Rev. Lett.* **126**, 246602 (2021).
- [15] G. Venturini, B. C. El Idrissi, and B. Malaman, *J. Magn. Magn. Mater.* **94**, 35 (1991).
- [16] B. Malaman, G. Venturini, R. Welter, J. Sanchez, P. Vulliet, and E. Ressouche, *J. Magn. Magn. Mater.* **202**, 519 (1999).
- [17] B. C. El Idrissi, G. Venturini, B. Malaman, and D. Fruchart, *J. Less-Common Met.* **175**, 143 (1991).
- [18] G. Venturini, D. Fruchart, and B. Malaman, *J. Alloys Compd.* **236**, 102 (1996).
- [19] T. Mazet, H. Ihou-Mouko, J. Marêché, and B. Malaman, *Eur. Phys. J. B* **51**, 173 (2006).
- [20] T. Mazet, G. Venturini, R. Welter, and B. Malaman, *J. Alloys Compd.* **264**, 71 (1998).
- [21] G. Kresse and J. Hafner, *Phys. Rev. B* **47**, 558 (1993).
- [22] G. Kresse and J. Furthmüller, *Comput. Mater. Sci.* **6**, 15 (1996).
- [23] G. Kresse and J. Furthmüller, *Phys. Rev. B* **54**, 11169 (1996).
- [24] H. J. Monkhorst and J. D. Pack, *Phys. Rev. B* **13**, 5188 (1976).
- [25] M. N. Ali, J. Xiong, S. Flynn, J. Tao, Q. D. Gibson, L. M. Schoop, T. Liang, N. Haldolaarachchige, M. Hirschberger, N. P. Ong, and R. J. Cava, *Nature* **514**, 205 (2014).
- [26] N. Nagaosa, J. Sinova, S. Onoda, A. H. MacDonald, and N. P. Ong, *Rev. Mod. Phys.* **82**, 1539 (2010).
- [27] Y. Tian, L. Ye, and X. Jin, *Phys. Rev. Lett.* **103**, 087206 (2009).
- [28] Y. Yao, L. Kleinman, A. H. MacDonald, J. Sinova, T. Jungwirth, D.-S. Wang, E. Wang, and Q. Niu, *Phys. Rev. Lett.* **92**, 037204 (2004).